Barrel swirl breakdown in spark-ignition engines: insights from particle image velocimetry measurements

M Reeves[1], **M J Haste**[2], **C P Garner**[2]* and **N A Halliwell**[2]
[1]Applied Optics Laboratory, Rover Group, Gaydon, Warwickshire, UK
[2]Department of Mechanical Engineering, Loughborough University, Leicestershire, UK

Abstract: Particle image velocimetry (PIV) has been used here to study the formation and breakdown of barrel swirl ('tumble') in a production geometry, four-stroke, four-valve, motored, spark-ignition, optically accessed internal combustion (IC) engine. The barrel swirl ratio (BSR) of the cylinder head could be enhanced by means of a port face inducer gasket so that the flow processes taking place at low and high swirl ratios could be investigated conveniently. Double-exposed images from planes both parallel and perpendicular to the cylinder axis were recorded at selected crank angles through the induction and compression strokes at a motored engine speed of 1000 r/min, with a wide open throttle, for both high and low BSR cases. The recorded images were interrogated by digital autocorrelation to give two-dimensional maps of instantaneous velocity.

In both high and low BSR cases, a barrel or tumbling vortex motion is generated during induction, which is shown to persist throughout the majority of the compression stroke. The details of barrel swirl formation during induction and its subsequent modification during compression, however, differ strongly between the two cases. These differences can be explained qualitatively in terms of two main events; the first being competition during induction between vortices of unequal strength and the second being competition between the large-scale swirl motion and the local flow field generated by piston motion during compression. In the low barrel swirl case, significant dissipation occurs owing to these interactions and consequently the large-scale motion exhibits lower mean velocities and undergoes significant distortion. In the case of high BSR, the competition effects are minimized and a single ordered vertical vortex exhibiting high velocity magnitudes is observed to avoid piston induced distortion. It then moves into the apex of the pent roof combustion chamber where it survives as a single ordered vortex until at least 40° crank angle (CA) before top dead centre (TDC). Limitations and developments of the PIV technique are discussed.

Keywords: engine, spark ignition, cylinder, fluid flow, PIV, swirl

NOTATION

BCL	bore centre-line (measurement plane)
BDC	bottom dead centre
BSR	barrel swirl ratio
°CA	degrees crank angle
CCD	charge coupled device
DBSR	dynamic barrel swirl ratio based on PIV measurements
IVC	inlet valve closure
LDV	laser Doppler velocimetry
PIV	particle image velocimetry
PTV	particle tracking velocimetry
$\boldsymbol{r}_i$	distance from centre of flow rotation to the ith vector point (m)
TDC	top dead centre
TVR	tumble vortex ratio
$\boldsymbol{v}_i$	velocity vector of the ith point in the vector map (m/s)
VCL	valve centre-line (measurement plane)
ω_e	engine crankshaft speed (rad/s)

The MS was received on 17 June 1998 and was accepted after revision for publication on 16 March 1999.
**Corresponding author: Department of Mechanical Engineering, Loughborough University, Loughborough, Leicestershire LE11 3TU, UK.*

1 INTRODUCTION

1.1 Motivation

Fluid motion within internal combustion (IC) engines fundamentally affects engine performance and emissions [**1**, **2**]. Modern multivalve spark-ignition engines with four valves per cylinder [**3**] exhibit favourable characteristics with regard to power output and exhaust emissions. This has been attributed in part to turbulence enhancement resulting from the breakdown of barrel or 'tumbling' motion, which is generated during the induction stroke [**4**]. As the piston approaches top dead centre (TDC) the large-scale tumble is believed to break down into relatively homogeneous microturbulence due to severe vortex distortion and shear. The enhanced turbulent flow field promotes rapid burn rate, improved flame propagation and better cyclic variability even under the high charge dilution conditions required for emissions control. Further, it has also been shown that significant charge dilution can be achieved in high barrel swirl engines by means of barrel charge stratification [**5**–**7**].

While turbulence enhancement is required for rapid and repeatable combustion of the charge, high barrel swirl ratios (BSR) may also produce strong bulk flows which, depending on the combustion chamber geometry, can persist throughout and after the time of ignition [**7**, **8**]. Excessive bulk flow may adversely affect initiation of the flame kernel owing to stretching of the arc discharge, or convection of the early flame kernel towards a combustion chamber wall. Additionally, excessive turbulence intensities may also lead to flame quenching owing to high local strain rates [**9**]. In the design of improved combustion systems it is therefore important to understand the evolution of the large scale in-cylinder flow structures, the phasing of their breakdown and how these processes are affected by the engine geometry, so that a suitable degree of turbulence enhancement can be achieved with minimal adverse effects on flame initiation and early flame growth.

For these reasons, advanced velocimetry techniques are being increasingly applied to the study and development of improved IC engines. Barrel swirl evolution in motored and fired engines has been studied using hot wire anemometry (HWA) [**3**] and laser Doppler velocimetry (LDV) [**10**–**12**] and these have provided much useful velocity and turbulence data at selected points within the flow field. However, the velocity fields are complex and unsteady and exhibit cyclic variations, so that whole field measurements are also required for full characterization of the in-cylinder flow. Hence whole field techniques such as particle tracking velocimetry (PTV) [**13**–**15**] and particle image velocimetry (PIV) [**16**, **17**] are finding increasing application in the study of in-cylinder flows. These closely related techniques are capable of providing instantaneous snapshots of unsteady velocity fields and have been reviewed by Adrian [**18**].

The use of high-energy pulsed laser illumination in PIV enables micrometre sized seeding particles to be used which are capable of following the rapid velocity fluctuations inherent in in-cylinder IC engine flows [**19**]. The technique is therefore well suited to the study of tumble breakdown in IC engines, giving quantitative flow field measurements prior to tumble breakdown and high resolution flow visualization of the turbulent eddy field thereafter. The high resolution imaging, which PIV entails, does, however, necessitate careful control of optical aberrations and optimization of the imaging system, flow seeding, illumination and interrogation parameters.

Internal combustion engine related PIV studies to date have included the measurement of motored [**20**] and fired [**21**] flows in high axial swirl engines, intake flow past an inlet valve [**22**] and cylinder wall ported engine flows under motored and fired conditions [**23**]. The authors have previously reported initial measurements of barrel swirl in a motored four-valve engine [**24**–**26**] and other similar work has been reported by Rouland *et al.* [**27**]. Further PIV measurements are presented here, mapping the evolution of barrel swirl throughout the induction and compression strokes in a production-geometry four-valve motored optical IC engine for low and high barrel swirl inlet configurations. High-resolution imaging of axial planes has been made possible by the development of a special corrective optical system that provides almost diffraction-limited imaging of particles within the thick glass cylinder. Experimental methods, which allowed routine acquisition of PIV images from the engine, are briefly described. A representative set of PIV data from horizontal and vertical planes within the cylinder are then presented and discussed. Finally, implications for future PIV engine studies and necessary refinements to the PIV technique are described.

1.2 Particle image velocimetry

Particle image velocimetry is now a well-established technique for the measurement of instantaneous planar velocity fields and has been reviewed by a number of authors [**18**, **28**, **29**]. In its simplest form, the flow is illuminated with a double pulsed light sheet and the positions of tracer particles are recorded with a photographic camera viewing normal to the plane of the sheet. The mean displacement vector of the particle images within each small region, divided by the laser pulse separation, gives the local flow velocity vector.

In this work, the two exposures were recorded on the same photographic film without image shifting [**18**] or colour labelling [**30**]. Standard autocorrelation analysis was then used to determine the mean velocity vector

within each small region of the flow, subject to a $\pm 180°$ ambiguity in the flow direction. However, in the case of this engine the large-scale tumble direction was known from previous LDV and flow visualization studies. The smaller-scale motions could be inferred from considerations of spatial and temporal flow continuity. Without *a priori* information such as this, a suitable means of image labelling such as two-colour recording [**30**] or high-speed digital recording [**31**] must be used to resolve directional ambiguity.

2 EXPERIMENTAL

2.1 Measurement conditions

Measurements were made on a single-cylinder four-stroke motored optical engine, designed and built by Advanced Power Train Technology, Rover Group. The four-valve, pent roof chamber engine was equipped with a piston crown and cylinder of fused silica. A schematic of the engine, showing optical access for axial (vertical) light sheets, is shown in Fig. 1. In this optical arrangement, the photographic camera would view the light sheet normal to its plane (i.e. into the paper). Measurements in horizontal planes could also be made by introducing a light sheet through the glass cylinder and viewing this through the piston crown window via the dielectric mirror.

The BSR of the cylinder head was determined by steady flow rig measurements using an impulse swirl meter as described by Chapman *et al.* [**32**]. This ratio relates the angular velocity of the tumbling flow in the steady flow rig to the equivalent crank rotation rate in a motored case. The steady flow BSR could be enhanced from the 'low' value of 1.2 to a 'high' value of 1.8 by means of an inlet port face inducer gasket. The gasket, shown schematically in Fig. 2, was mounted between the inlet manifold and the inlet port face to

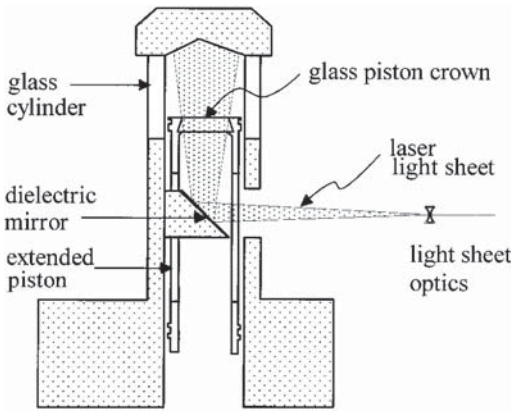

Fig. 1 Schematic of the single-cylinder optical engine showing access for vertical light sheets (crankshaft and connecting rod assembly not shown)

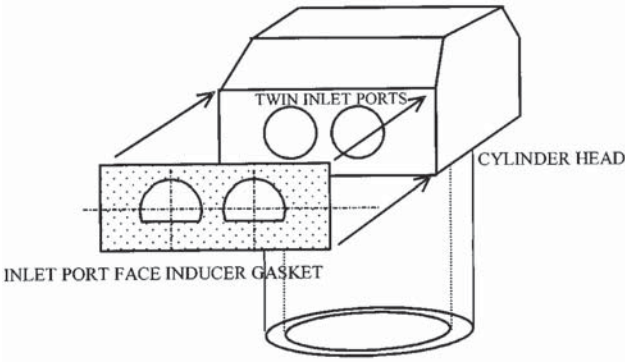

Fig. 2 Inlet port face inducer gasket

mask off the lower portion of the twin inlet ports. The mask was designed experimentally to increase the BSR as measured on the steady flow rig without significantly reducing the flowrate. Pressure traces recorded from the motored engine with and without the port face inducer confirmed that the flow structure was modified without compromising cylinder pressure at the measurement speed.

For this study the engine was motored at a crank speed of 1000 r/min with a wide open throttle (WOT). The engine configuration and operating condition are summarized in Table 1.

2.2 Measurement locations

Results from three measurement planes are presented here; two parallel vertical (axial) planes and a single horizontal (radial) plane. The vertical planes were both parallel to the cylinder head symmetry plane and were chosen to study the predominantly in-plane tumbling motion. The valve centre-line (VCL) plane passed through the centre of an inlet and exhaust valve, the bore centre line (BCL) plane being the symmetry plane passing through the cylinder and spark plug centre-line (see Fig. 3).

A single horizontal plane was chosen to characterize the compression flow field at the time of ignition. The horizontal plane was located 3 mm below the cylinder head face, which placed it approximately 10 mm below the lower face of the spark plug electrode. Owing to strong tumbling motion, the flow in the horizontal

Table 1 Engine configuration

Bore (mm)	84.45
Stroke (mm)	89
Swept volume (cm^3)	500
Compression ratio	10.5:1
Valve lift (mm)	10.16
Inlet valve peak lift	70°CA before BDC
Exhaust peak lift	70°CA after BDC
Cam period	240°CA
Engine speed (r/min)	1000

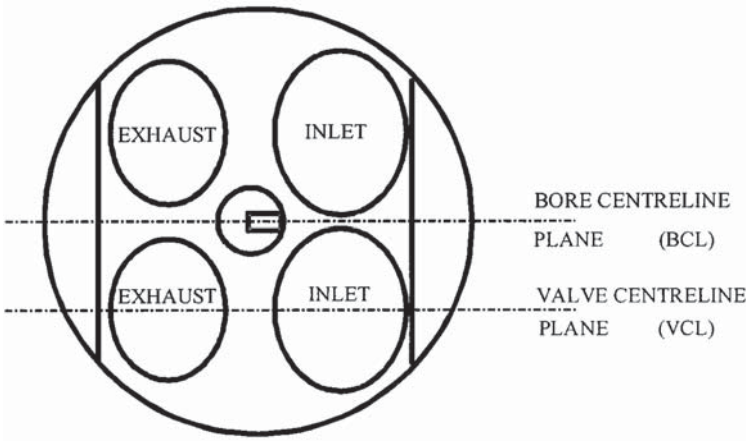

Fig. 3 Location of vertical (axial) measurement planes

plane generally has a high out-of-plane component at arbitrary crank angles and thus measurements are only presented at the nominal ignition point of 338° after TDC. At this crank angle, the flow is significantly in-plane owing to the favourable aspect ratio of the clearance volume and the proximity of the piston crown. The horizontal plane was viewed via the 45° mirror and piston crown window (see Fig. 4), whereas the vertical plane was viewed through the wall of the fused silica cylinder.

The range of crank angles and measurement planes for which PIV results are presented is given in Table 2. The challenges associated with measurement in each location and crank angle are discussed later in Section 4.

2.3 Experimental techniques

Many of the experimental techniques that follow have been described in earlier publications [**24**, **25**, **33**]. However, a brief overview of the PIV engine facility and essential experimental techniques is given here for completeness. The complete facility is shown schematically in Fig. 5 and consists of several subsystems. These include the illumination system, the optical engine, flow seeding equipment, imaging equipment and some special diagnostic tools to align the laser sheets, monitor the seed density and achieve accurate camera focusing.

2.3.1 Light sheet formation

A frequency doubled, dual oscillator, dual amplifier Spectron Nd:YAG system gave individual pulses of 8 ns duration with pulse energies of approximately 100 mJ at a wavelength of 532 nm. The laser pulse separation could be infinitely varied and the pulses could be synchronized with the engine crank position to a resolution and repeatability of 0.1°CA.

The laser output was formed into a collimated sheet approximately 600 μm thick, using a 200 mm focal length positive cylindrical lens and a -30 mm focal length biconcave spherical lens. Precise overlap of the two laser sheets was determined by measuring their intensity profiles using a pinhole and photodetector assembly. In this way, intensity profiles were measured at three points along the sheet centre-line and adjustments were performed until the beam centres coincided to ± 50 μm. Intensity profiles recorded with and without Pockels cell operation showed that the position of the beams was not significantly affected by Q-switching. This allowed low-power, non-Q-switched beams to be used reliably for safe and accurate beam alignment.

The vertical sheets were introduced through the piston crown via a dielectric mirror, thereby minimizing stray reflections. Datum plates located on machined engine faces were used to position the sheets to an accuracy of ± 0.25 mm over the measurement region. The horizontal sheet was introduced as close to the head gasket as flare allowed, while just missing the

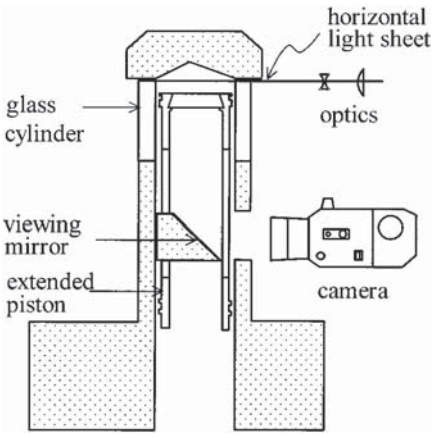

Fig. 4 Engine schematic showing access for horizontal light sheets

Table 2 Measurement crank angles and locations

°CA after TDC inlet	Significance	Measurement planes
222	Inlet valve closure	VCL
260	Intermediate point	VCL
300	Expected swirl breakdown for low BSR head	VCL, BCL
320	Intermediate point	VCL
338	Nominal ignition point	VCL, horizontal

piston crown surface at TDC. This sheet was located accurately using the piston crown surface as a datum plane. Levels of flare were generally much higher for the horizontal planes than for the vertical planes owing to multiple reflections within the glass cylinder and consequent illumination of the combustion chamber walls.

2.3.2 *Flow seeding*

A Laskin atomizer was used to generate a fine mist of 0.5–2.0 μm silicone oil droplets. The seed was introduced into the intake plenum of the engine to achieve uniform mixing. The seed density was controlled by the air supply pressure to the atomizer using a precision low-pressure regulator. The optimum density of particle images for autocorrelation PIV is known to be approximately 15–25 particle image pairs per interrogation region where strong velocity gradients are present [**34**]. The appropriate seed density was achieved consistently within the engine by monitoring the side-scattered laser light intensity using a 100 mm^2 silicon photovoltaic detector mounted in the camera viewfinder, which gave a voltage output proportional to the seed density in the centre of the field of view as the laser was pulsed. The integrated voltage output from the detector was calibrated against the particle image density measured in PIV images recorded at inlet valve closure (IVC). Reoptimization of the seed density for crank angles closer to TDC was achieved by reducing the density measured at IVC by a factor appropriate to the compression at the measurement crank angle.

2.3.3 *Photographic techniques*

A medium-format Mamiya 645 camera with a Mamiya Sekor f4 80 mm macrolens was used at an aperture of $f\# = 5.6$ and a magnification of 0.4, producing particle images of 10–20 μm in diameter over fields of view up to 60 mm wide and 95 mm high. The depth of field was approximately 0.8 mm. Kodak Technical Pan 2415 film was developed with D-19 to give a speed of around 100 ASA at a resolution of approximately 200 line pairs/mm. A Balzers additive dichroic colour filter having a bandpass of approximately 60 nm centred at 540 nm was mounted in front of the camera lens to block background light. This allowed the engine to be run and images to be recorded under safe room-lit conditions, with shutter periods of up to 1 s.

Accurate camera focusing was achieved using a technique described by Hocker and Kompenhans [**35**]. A

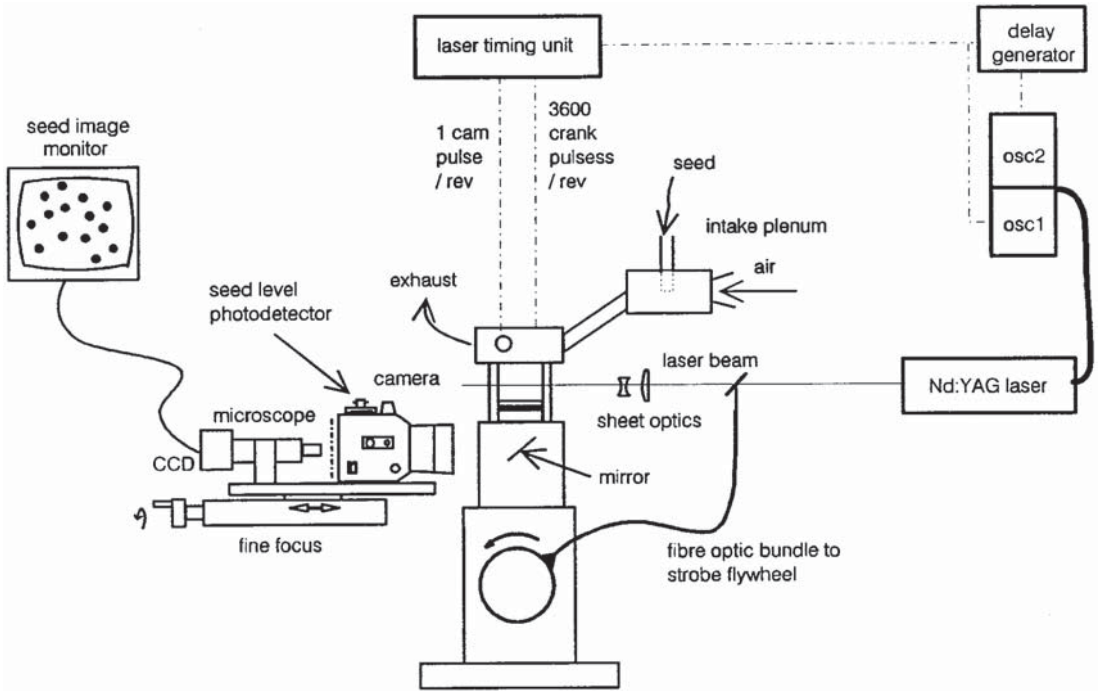

Fig. 5 Schematic of PIV engine facility

microscope imaged a small region of the camera image plane on to a CCD array, allowing a highly magnified view of the region to be displayed on a monitor (Fig. 5). The quality and density of live particle images in any region of the film plane could then be assessed and optimized. This procedure was essential in ensuring that the camera film plane was accurately parallel with the horizontal film plane. The camera lens was operated at fixed focus to eliminate the need for repeated calibration of magnification. Focusing was performed by translating the camera and microscope assembly on coarse and fine translation stages. The CCD microscope arrangement was employed to optimize the complete imaging system for the plane of interest prior to PIV measurements. Once focusing was complete, the microscope could be removed and the loaded film cassette clipped in place.

Highly aberrated particle images were formed when vertical sheets were viewed through the glass cylinder. A special corrective optical system was therefore developed which was placed between the camera lens and the engine cylinder and allowed high-quality particle images to be formed. The particle images were almost diffraction-limited close to the centre of the field of view of the camera. The particle image diameter degraded from approximately 12 μm at the optical axis to 20 μm at a distance of 10 mm from the cylinder wall. The performance and design of this system are discussed in detail in references [**26**] and [**33**].

2.3.4 Interrogation of images

Images were interrogated on a square grid with 50 per cent overlap between neighbouring interrogation regions, using a commercial digital autocorrelation system developed by AEA Harwell. An autocorrelation resolution of 256×256 was used and for each interrogation region the location of the centroids of the three highest signal peaks were recorded. Raw vector maps consisted of vectors derived from the highest signal peak in each region. These were then edited by removal of all vectors above and below sensible maximum and minimum velocity thresholds and remaining vectors that showed gross discontinuity with neighbours were replaced by second or third candidates, or removed entirely if no appropriate choice could be made. Data dropout occurred in regions where the velocity was smaller than the lower extreme of the dynamic range (~ 3 m/s), where velocity gradients and out-of-plane velocities were excessive and where stray light or 'flare' caused excessive background image noise [**33**]. Limited interpolation, based on mass continuity, was applied where necessary.

3 RESULTS AND DISCUSSION

The PIV images obtained could provide a vector grid spacing of 0.5×0.5 mm, but this was considered too fine for adequate whole-field reproduction in this paper. Therefore, in the vector maps that follow, the vectors are plotted on a coarse grid of 2.2×2.2 mm for clarity. However, the important features of the flow are preserved whichever grid spacing is used. The direction of the predominant swirl over the piston crown at IVC has been assumed from previous Rover flow visualization and LDV studies that revealed the direction of the single large-scale tumble vortex to be anticlockwise. The initial rotational sense of the main barrel vortex is subsequently maintained throughout the stroke until close to the ignition point. Strictly, the direction of flow vectors within smaller-scale flow structures is subject to the usual 180° ambiguity inherent in autocorrelation analysis. In the results that follow, the position of the piston crown at the measurement crank angle is shown as a thick horizontal line beneath the measurement region.

3.1 Induction flow field

The induction flow fields within IC engines are characterized by a large velocity dynamic range and high velocity gradients and are best suited to cross-correlation PIV. However, Figs 6a and b are able to show the main features of the induction flow fields in the VCL plane at a crank angle of 45° after TDC. In the low barrel swirl case in Fig. 6a, the flow over the top of the inlet valve sets up a rapidly rotating vortex beneath the exhaust valve. This is accompanied with a counter rotating vortex of similar size beneath the inlet valve, and a strong vertical 'fountain' flow between the two vortices near the cylinder axis. In the high barrel swirl case in Fig. 6b, the flow over the top of the inlet valve dominates the flow issuing from the bottom of the valve, and a single ordered vortex located more centrally within the cylinder dominates a much weaker counter-rotating vortex beneath the inlet valve. The net angular momentum in the high BSR flow is therefore higher and gives rise to a simple and strongly ordered flow after the time of inlet valve closure.

3.2 Compression flow field

3.2.1 Vertical VCL plane

The flow in the VCL plane during compression for the high and low BSR inlet systems is shown in Figs 7, 8, 9a and b. At all crank angles during compression, the maximum flow velocities are higher for the 1.8 BSR case and the results show significant

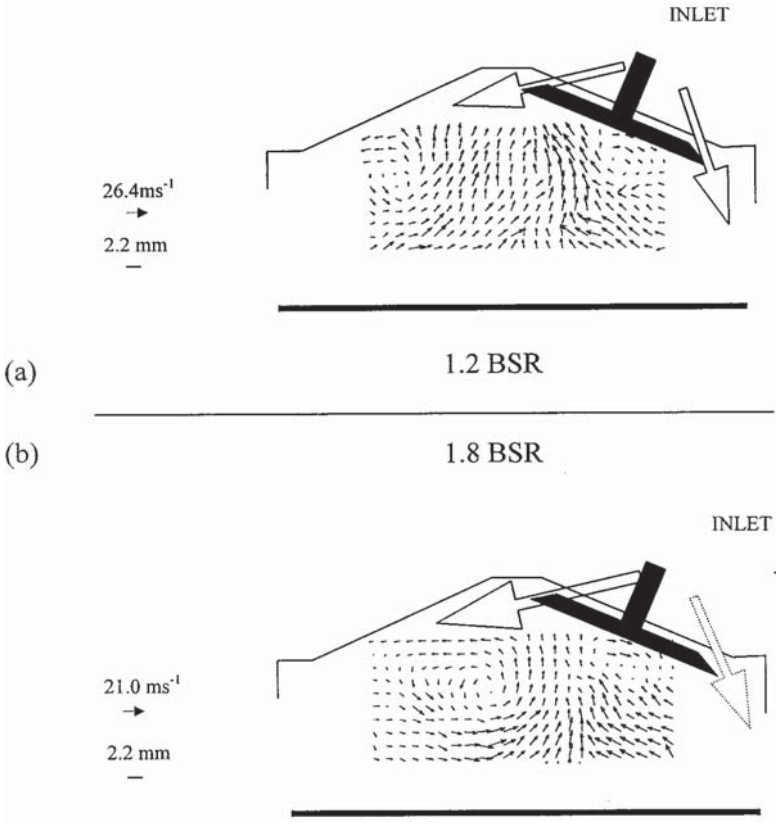

Fig. 6 PIV velocity vector maps of the in-cylinder flow during induction in the VCL plane for (a) BSR = 1.2 and (b) BSR = 1.8 (45°CA after TDC inlet)

differences in the flow processes that lead to barrel swirl breakdown.

At IVC (i.e. 222°CA after TDC) an ordered barrel vortex is seen in both low and high BSR cases (Figs 7a and c). However, the maximum velocities in the high BSR flow are approximately 1.75 times higher than in the low BSR case. This is in reasonable agreement with the steady flow BSR values for the high and low configurations, which are in a ratio of 1.5:1.

An important point is that the flow fields at IVC are far from solid body rotations. In fact, the flow contains regions of high momentum that penetrate the cylinder volume over time. Therefore, the spatial distribution of linear and angular momentum is not uniform, a fact which has implications for the effects of piston motion later on during compression. In the low swirl case, at IVC the region of highest velocity (sometimes known as the 'swirl tongue') has progressed towards the top right of the measurement area, beneath the inlet valve in Fig. 7a. In the high BSR case, the highest-velocity air has already penetrated the combustion chamber and is issuing downwards from beneath the exhaust valve to complete a full circuit of the measurement area (Fig. 7c).

By 260°CA after TDC in the high BSR case, a single barrel vortex is seen whose rotation centre is positioned close to the geometrical centre of the clearance volume (Fig. 7d). The maximum velocities have increased slightly, which may be evidence of 'spin-up'. In contrast, the low BSR flow field at 260°CA (Fig. 7b) shows a tumbling motion without a single clear centre of rotation. The maximum velocity remains unchanged from the previous crank angle.

By 300°CA after TDC, the flow in the high and low BSR cases are profoundly different (Figs 8a and c). At this crank angle, the piston has moved past its position of maximum instantaneous speed. In the low BSR case (Fig. 8a) the piston motion has been sufficient to stagnate and reverse the flow to the exhaust port side of the piston crown. As a consequence, the barrel swirl motion undergoes significant distortion and can no longer be described as an ordered tumbling vortex. The high shear forces generated by the distortion process imply that significant dissipation of large-scale rotational energy must be taking place at this relatively early stage in compression. In the high BSR case (Fig. 8c) the flow velocities are always higher than the maximum piston speed. Consequently, the stagnation process above the left-hand face of the piston crown does not dominate the evolution of the flow and the relatively undistorted vortex can move easily into the apex of the pent roof clearance volume without significant distortion.

At 320°CA after TDC, a single, fairly symmetrical barrel vortex is still seen in the high BSR case (Fig. 8d). In the low BSR case at the same crank angle, the flow has become more complex (Fig. 8b). Owing to directional ambiguity, caution is required in the interpretation of this velocity map, especially in the region immediately beneath the exhaust valve where some vectors have been omitted because of uncertainties in their direction. However, it is clear that the barrel vortex has been forced over beneath the inlet valve and that a strong reverse flow has been set up beneath the exhaust valve. With the barrel vortex centre located in this position, further compression must lead to further rapid distortion and early turbulence generation compared with the high BSR case.

The optical access available at the ignition crank angle (338°CA after TDC) is limited and only a thin slice of the flow field may be observed at this stage. For

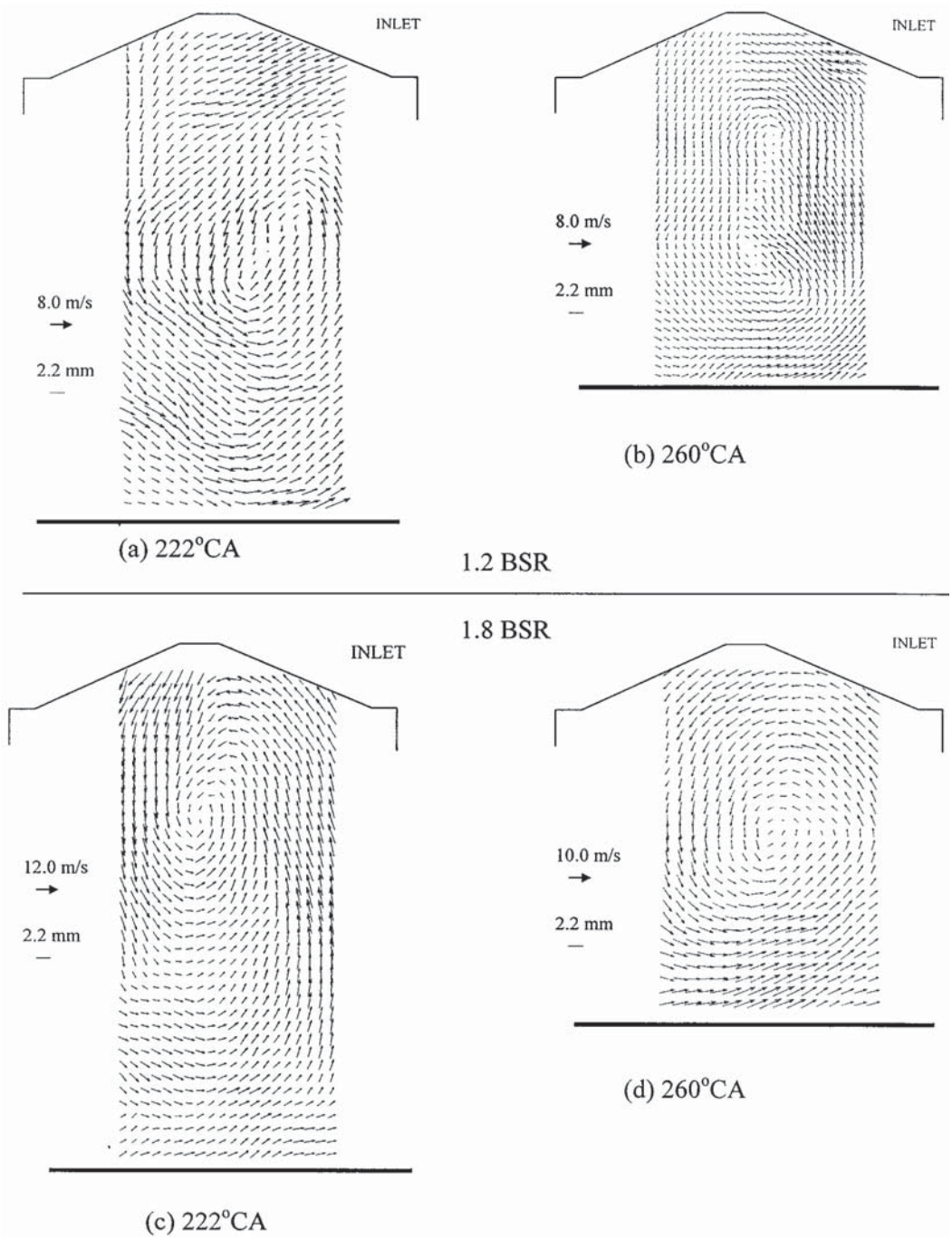

Fig. 7 PIV velocity vector maps of the in-cylinder flow in the vertical VCL plane for (a, b) BSR = 1.2 and (c, d) BSR = 1.8 (222 and 260°CA after TDC inlet)

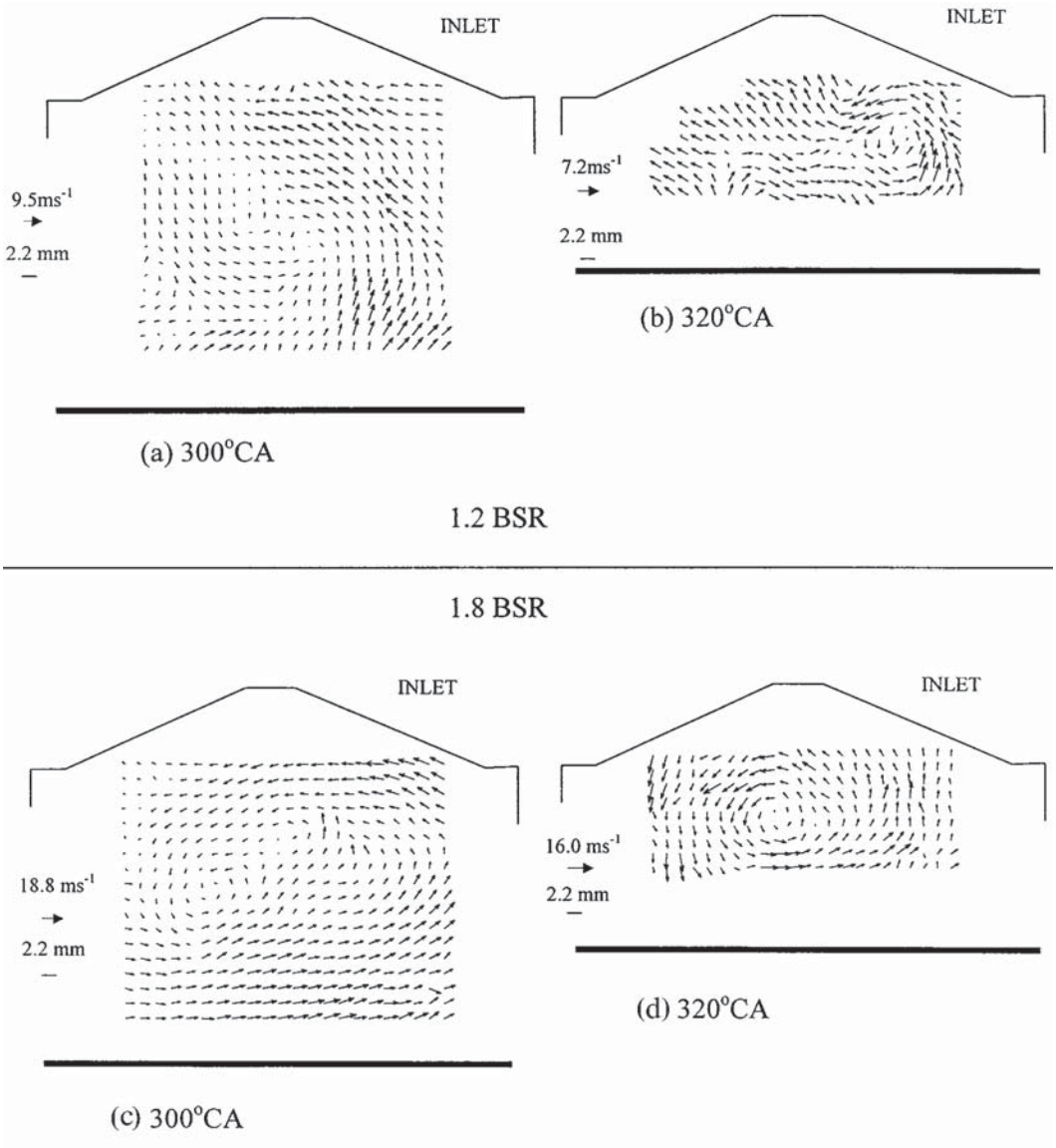

Fig. 8 PIV velocity vector maps of the in-cylinder flow in the vertical VCL plane for (a, b) BSR = 1.2 and (c, d) BSR = 1.8 (300 and 320°CA after TDC inlet)

this reason, firm conclusions about the flow structure in the combustion chamber close to ignition cannot be drawn with certainty. However, the results of Figs 9a and b show that there remain some interesting differences between the high and low BSR cases. In the high BSR case (Fig. 9b) the maximum velocities are higher and the flow appears more organized than in the low BSR case (Fig. 9a). In both instances the flow velocities in the roof of the combustion chamber are in the range 10–15 m/s. If these velocities scale linearly with engine speed, bulk velocities in the combustion chamber could exceed those required adversely to affect the spark discharge and early flame kernel in a firing engine.

3.2.2 *Horizontal plane*

The flow at the nominal ignition point of 338°CA after TDC was also recorded in the horizontal plane located 3 mm down from the cylinder head face. This placed the measurement plane several millimetres below the vertical region shown in Figs 9c and d. Difficulties were encountered in achieving a uniform light sheet across the whole cylinder, owing to seeding fluid deposited by the piston rings at TDC and light sheet divergence. The results shown in Figs 9c and d are therefore given only in the cylinder half-plane closest to the illumination source where the appropriate light sheet quality could be achieved.

Figure 9d shows a horizontal cross-section through

the so-called 'wing vortices' previously observed by Kuwahara *et al*. [7] in a similar engine. In the high swirl case (Fig. 9d) the vortices exhibit higher velocities and a stronger circulation than in the low BSR case (Fig. 9c). The presence of a strong in-plane horizontal motion demonstrates that the velocity field has become significantly three-dimensional at this crank angle. This is due to the rapidly changing aspect ratio of the clearance volume, which can no longer support a purely tumbling flow field, and the close proximity of the piston crown to the measurement plane.

3.2.3 *Vertical BCL plane*

Measurements on the BCL plane towards the end of the compression stroke were problematic owing to flare from the spark plug and combustion chamber surfaces. High quality PIV images were, however, recorded at the

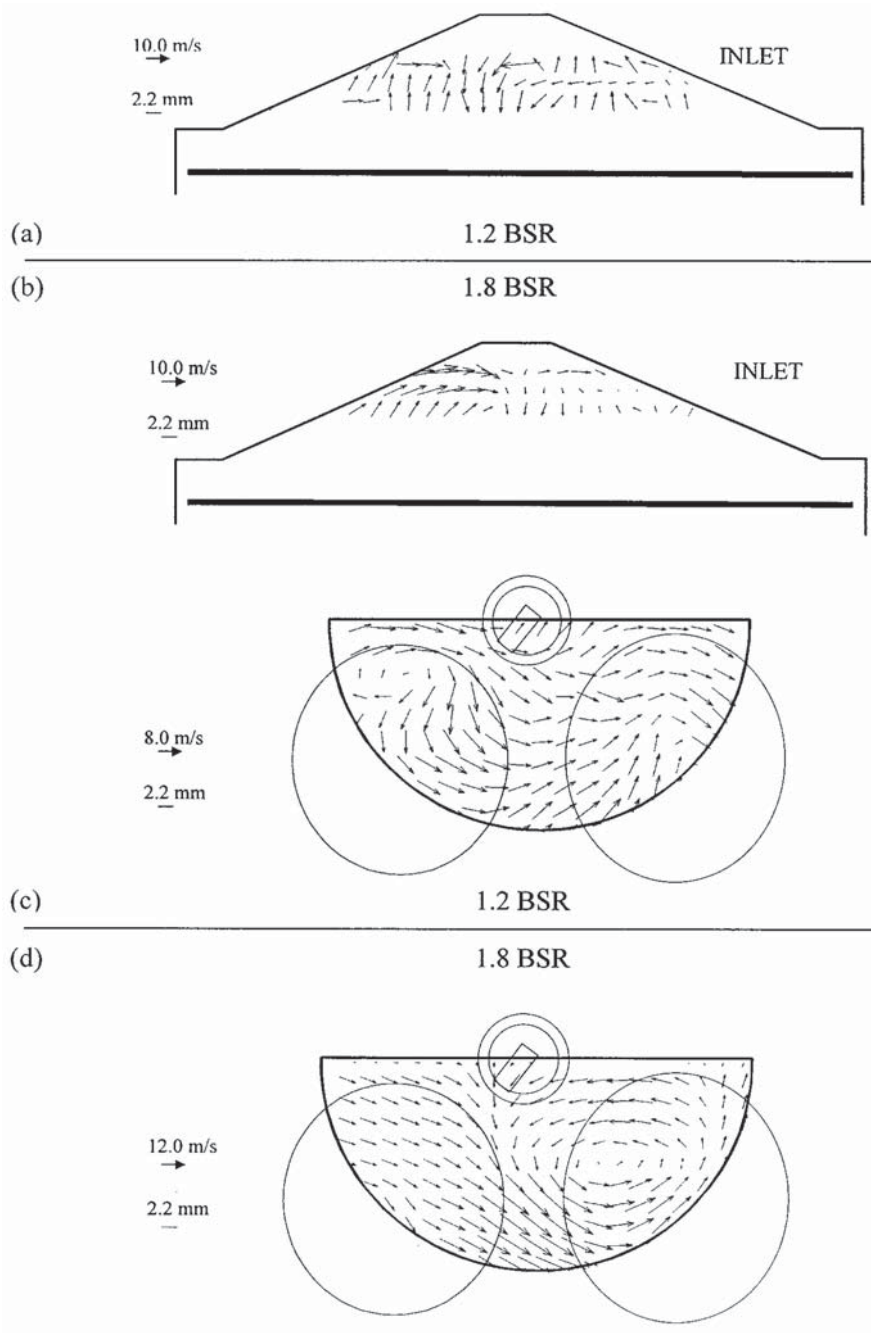

Fig. 9 PIV velocity vector maps of the in-cylinder flow in (a, b) the vertical VCL plane and (c, d) the horizontal plane for both BSR = 1.2 and 1.8 (ignition point 338°CA after TDC inlet)

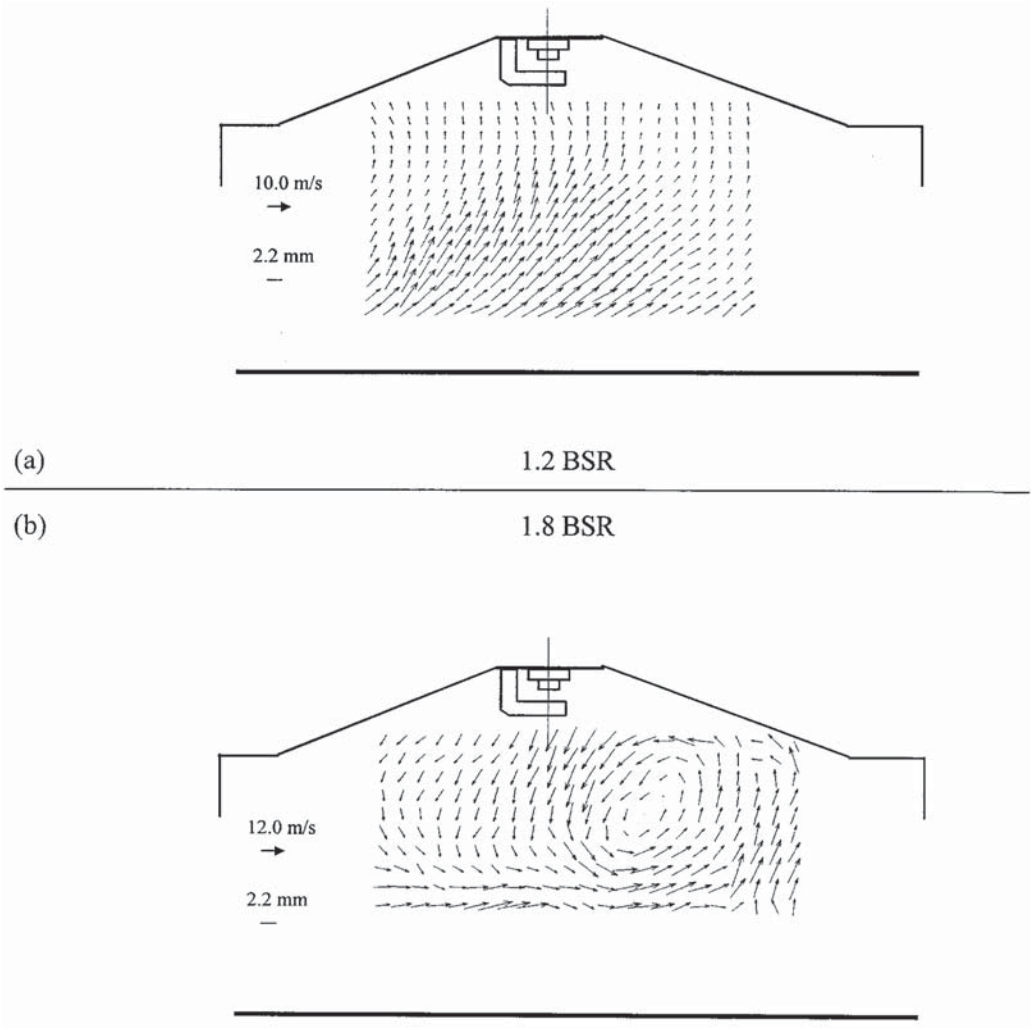

Fig. 10 PIV velocity vector maps of the in-cylinder flow in the vertical BCL plane for (a) BSR = 1.2 and (b) BSR = 1.8 (300°CA after TDC inlet)

300°CA and these were sufficient to illustrate significant differences in the flow behaviour on the VCL and BCL planes and the potential for high-velocity bulk flows in the region of the central spark.

The flow fields at 300°CA after TDC for the low and high swirl heads are shown in Figs 10a and b respectively. In the low BSR case, the flow appears to be a simple bulk motion with a flow angle of approximately 45°. There is no evidence of vortex motion within the measurement region. This is in contrast to the high BSR case (Fig. 10b), which clearly shows a large-scale barrel vortex whose centre is biased towards the inlet port.

By comparing the flow at 300° CA in the two vertical measurement planes, some limited information about the three-dimensional flow behaviour for the two BSR cases can be gained. In the high BSR, both measurement planes show a similar simple vortical structure (see Figs 10b and 8c). This in contrast to the low BSR case, in which the flow field is radically different in the two planes (see Figs 10a and 8a). In this sense, it is clear that the low BSR flow field at this crank angle is distinctly less ordered and more three-dimensional than in the high BSR case.

3.3 Barrel vortex 'spin-up'

Descriptions of barrel swirl behaviour during the latter stages of compression often refer to a period of vortex 'spin-up'. This is an increase in rotation rate owing to conservation of angular momentum as the flow field is forced into the reducing clearance volume near TDC. By analogy with the steady flow barrel swirl ratio, a dynamic BSR or 'tumble vortex ratio' (TVR) can be calculated at each measurement crank angle from LDV or PIV datasets as described by Hu [**8**]. This ratio relates the mean angular velocity determined from the velocity field to the angular velocity of the engine crank. An increase in this value during compression is cited as evidence for vortex 'spin-up'.

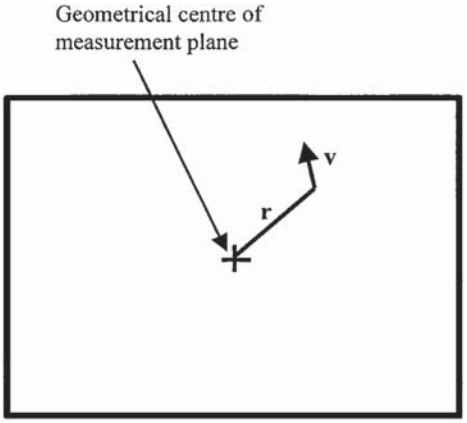

Fig. 11 Geometry for calculation of DBSR in the velocity plane

For the general rotating flow field, the barrel swirl ratio from planar velocity data is estimated by summation of the angular momentum of each velocity vector about the centre of rotation. Taking the magnitude of this vector summation and dividing by the moment of inertia of the flow gives the equivalent solid body rotation rate. Dividing this by the crank rotation rate of the engine gives the non-dimensional dynamic barrel swirl ratio (DBSR) as

$$\mathrm{DBSR} = \frac{\left|\sum_i^N \boldsymbol{v}_i \wedge \boldsymbol{r}_i\right|}{\omega_e \sum_i^N \boldsymbol{r}_i \cdot \boldsymbol{r}_i} \tag{1}$$

where $\boldsymbol{v}_i$ is the ith velocity vector in the PIV velocity vector map, ω_e is the angular velocity of the engine crankshaft and $\boldsymbol{r}$ is the vector distance of the measurement point from the centre of the flow field as illustrated in Fig. 11.

PIV-based DBSR results were obtained for 220–320°CA after TDC and both the VCL and BCL planes for both the low- and high-impulse swirl meter measurement-derived BSRs of 1.2 and 1.8 respectively. These are shown in Figs 12a and b. In the case of the low BSR head, the behaviour of the DBSR with crank angle is dependent

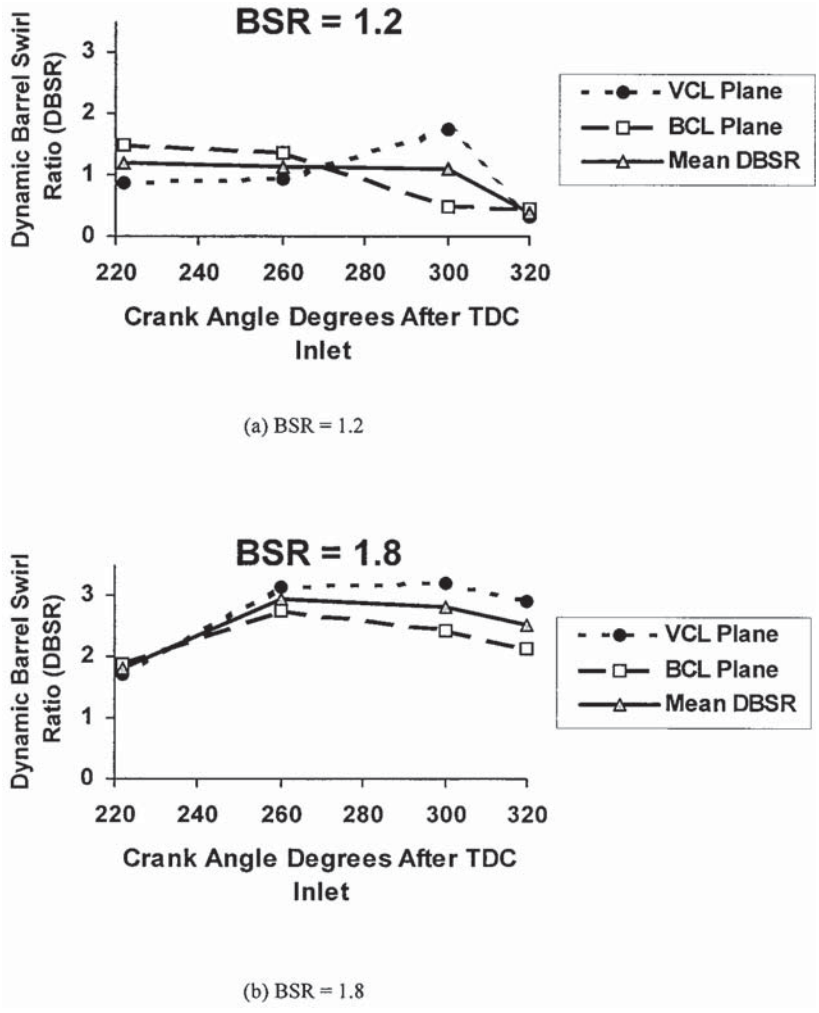

Fig. 12 Dynamic barrel swirl ratio as a function of the engine crank angle for (a) BSR = 1.2 and (b) BSR = 1.8

on the measurement plane. The mean DBSR value at IVC is 1.2, this being equal to the nominal steady flow BSR value. The BCL plane first demonstrates a higher DBSR than the VCL plane, but this is reversed after 260°CA. With reference to the original PIV velocity maps, the flow structure on the BCL plane is significantly different to that on the VCL plane at the low BSR (1.2) condition, so the flow cannot be considered as a simple two-dimensional barrel vortex. Linear and angular momentum will be transferred from one plane to another as the high-velocity swirl 'tongue' moves in three dimensions around the cylinder. The low DBSR at 320°CA after TDC indicates that by this stage any large-scale rotational motion has largely disappeared. However, this does not necessarily imply that velocities are low or that turbulent breakdown is complete; bulk convective motion of the kind seen in the BCL plane at 260°CA after TDC will give rise to a low DBSR but high mean velocities.

In the high BSR case (BSR = 1.8) the behaviour of the DBSR is similar for both vertical planes as shown in Fig. 12b. This is indicative of a more organized two-dimensional barrel vortex in which the gas rotates in a more organized fashion. The mean DBSR at IVC is 1.7, this comparing favourably with the impulse swirl measurement of 1.8. It appears, therefore, that the steady flow BSR technique described by Chapman *et al.* [**32**] is indeed suitable for the characterization of the initial in-cylinder DBSR at IVC. The mean DBSR value is first seen to rise after IVC to a maximum of approximately 3.0 at 260°CA after TDC and then decays slowly towards 320°CA.

4 FURTHER IMPROVEMENTS TO PIV

The ability to record PIV images routinely from both horizontal and vertical planes within a realistic geometry engine has been demonstrated. Further, the application of PIV to the study of in-cylinder flow has yielded useful whole-field flow visualization and quantitative data that are complementary to the detailed statistical data obtained using the more conventional hot wire anemometry and LDV techniques. If, however, full use is to be made of the potential of PIV, improvements in the technique are required. These include the need to reduce the effects of flare, or stray light, in the images, the need to resolve directional ambiguity and the need to expand the measurement dynamic range while reducing data dropout due to high-velocity gradients.

The problem of flare may be reduced by using larger seeding particles. In particular, the use of hollow spherical particles a few micrometres in diameter should allow similar flow-following fidelity to the smaller oil droplets used in this study, with an order of magnitude increase in the side scattered intensity [**36**]. An alternative approach to stray light rejection, using fluorescent seed particles, has also been demonstrated [**37**]. The effects of stray light may be further reduced at the interrogation stage by appropriate morphological filtering [**38**].

Directional ambiguity is inherent in simple twin-exposure PIV recording but may be eliminated by various means including image shifting, image separation [**39**] and image labelling [**40**, **41**]. Various image shifting techniques have been shown to be beneficial in many applications [**42**–**45**], and these may be adapted for cross-correlation analysis [**46**]. Cross-correlation interrogation has a number of significant advantages over autocorrelation. Firstly, the number of spurious correlation peaks is reduced compared with autocorrelation and this provides a significant increase in the proportion of valid signal peaks that are detected. Also, since there is no large central peak in cross-correlation, the lower end of the velocity dynamic range is extended to velocities approaching zero. It can further be shown that a proportion of this expanded velocity dynamic range can be traded for increased tolerance to velocity gradients by reduction in the maximum permitted particle displacement [**24**, **47**]. For these reasons, cross-correlation is not merely desirable but an essential development for application of PIV in complex flows. Recent examples of successfully implemented cross-correlation PIV for routine engine studies include: cycle-resolved measurements using electronic imaging [**31**], two-colour image-labelled photographic PIV [**30**] and birefringent image-shifted photography [**48**].

5 CONCLUSIONS

1. The evolution of barrel swirl in a realistic geometry pent roof four-valve motored engine, from BDC through to the ignition point, has been studied using PIV. Measurements were possible in both horizontal and vertical planes at low and high barrel swirl ratios.
2. There is good correlation between the broad features of the PIV results and the LDV, hot-wire and particle tracking measurements performed by other workers in similar engine geometries. Large-scale motion is preserved throughout compression up to the ignition point, giving high-velocity bulk flow in the combustion chamber roof at the time of ignition. This is especially true at the higher BSR.
3. The DBSR results show little evidence for significant vortex 'spin-up'. The variation in the DBSR behaviour with measurement plane for the low BSR case indicates that the flow is less ordered and more three-dimensional than for the high BSR case for the majority of the compression stroke. In both cases, after IVC, high-momentum gas moves around the cylinder volume in a transient process, in which the mean flow velocity increases little throughout compression.

4. The major differences in the flow evolution between two BSR cases can be explained in terms of three important phenomena:
   (a) competition between opposing vortices of differing strength during induction,
   (b) competition between piston-induced motion and the post-induction flow field,
   (c) the ability of the clearance geometry to accommodate the flow pattern caused by (a) and (b).
5. Improvements in optical access and flare reduction are required to permit detailed study of the ignition flow field in vertical planes. The ability to measure the flow close to spark will permit a detailed study of the effects of local flow on ignition and flame kernel growth and assist optimization of combustion chamber geometry.
6. Use of cross-correlation is required for improved PIV measurements, resolving directional ambiguity, expanding dynamic range, improving signal–noise ratio and increasing spatial resolution and tolerance to velocity gradients.

ACKNOWLEDGEMENTS

The authors would like to thank a number of people for their assistance in this work. Dr Jeremy Coupland at Loughborough University for valuable advice; Steve Retter at Loughborough University, for the design and build of the electronic timing system; the engine design, build and optical teams at Rover: Graham Marshall, Peter Parker, Trevor Wood, Adrian Fitzpatrick (especially for the steady flow measurements), Stan Wallace, Dr Jeremy Davies and Dr Clive Buckberry; funding by Rover Group and the UK Engineering and Physical Sciences Research Council (Grant GR/G55426).

REFERENCES

1 **Arcoumanis, C.** and **Whitelaw, J. H.** Fluid mechanics of internal combustion engines: a review. *Proc. Instn Mech. Engrs*, *Part D*, *Journal of Automobile Engineering*, 1987, **201**(D1), 57.
2 **Heywood, J. B.** Fluid motion within the cylinder of internal combustion engines—the 1986 Freeman Scholar Lecture. *Trans. ASME*, *J. Fluids Engng*, 1987, **109**, 3.
3 **Benjamin, S. F.** The development of the GTL 'barrel swirl' combustion system with application to four-valve spark ignition engines. IMechE paper C54/88, 1988, p. 203.
4 **Arcoumanis, C., Hu, Z., Vafidis, C.** and **Whitelaw, J. H.** Tumbling motion: a mechanism for turbulence enhancement in spark-ignition engines. SAE paper 900060, 1990.
5 **Kiyota, Y., Akishino, K.** and **Ando, H.** Concept of lean combustion by barrel stratification. SAE paper 920678, 1992.
6 **Baritaud, T. A.** Optical and numerical diagnostics for SI engine combustion studies. In Proceedings of COMODIA 94 Conference on *Combustion Diagnostics and Modelling in IC engines*, Yokohama, Japan, July 1994.
7 **Kuwahara, K., Watanabe, T., Takemura, J., Omori, S., Kume, T.** and **Ando, H.** Optimisation of in-cylinder flow and mixing for a centre-spark four-valve engine employing the concept of barrel-stratification. SAE paper 940986, 1994.
8 **Hu, Z.** Turbulence enhancement in spark-ignition engines. PhD thesis, Imperial College of Science, Technology and Medicine, London, 1992.
9 **Bradley, D.** and **Sheppard, C. G.** Limitations to turbulence enhanced burning rates in lean burn engines. IMechE paper C46/88, 1988.
10 **Witze, P. O.** A critical comparison of hot-wire anemometry and laser Doppler velocimetry for I.C. engine applications. *Trans. SAE*, 1980, **89**, paper 800132, 711.
11 **Hu, Z., Vafidis, C., Whitelaw, J. H., Chapman, J.** and **Head, R. A.** Correlation between in-cylinder flow, performance and emissions characteristics of a Rover pentroof four-valve engine. IMechE paper C448/026, 1992, p. 157.
12 **Hadded, O.** and **Denbratt, I.** Turbulence characteristics of tumbling air motion in four-valve S.I. engines and their correlation with combustion parameters. SAE paper 910478, 1991.
13 **Khaligi, B.** Intake-generated swirl and tumble motions in a 4-valve engine with various intake configurations—flow visualisation and particle tracking velocimetry. In Proceedings of SAE Congress and Exposition, Detroit, 1990, paper 900059, 1990.
14 **Ronnback, M., Le, W. X.** and **Linna, J.-R.** Study of induction tumble by particle tracking velocimetry in a 4-valve engine. *Trans. SAE*, 1991, paper 912376.
15 **Rimai, L., Adamczyk, A. A., Mikulec, A. and Kent, J. C.** Quantitative three-dimensional reconstruction of flow fields from orthogonal views of particle tracks: application to a water analog of a piston engine. In Proceedings of 5th International Symposium on *Flow Visualisation*, Prague, Czechoslovakia, 1989.
16 **Pickering, C. J. D.** and **Halliwell, N. A.** Speckle photography in fluid flows: signal recovery with two-step processing. *Appl. Optics*, 1984, **23**, 1128–1129.
17 **Adrian, R. J.** Scattering particle characteristics and their effect on pulsed laser measurements of fluid flow: speckle velocimetry *vs* particle image velocimetry. *Appl. Optics*, 1984, **23**, 1690–1691.
18 **Adrian, R. J.** Particle imaging techniques for experimental fluid mechanics. *Annual Rev. Fluid Mech.*, 1991, **23**, 261–304.
19 **Haghgooie, M., Kent, J. C.** and **Tabaczynski, R. J.** Verification of LDA and seed generator performance. *Experiments in Fluids*, 1986, **4**, 27–32.
20 **Reuss, D. L., Adrian, R. J., Landreth, C. C., French, D. T.** and **Fansler, T. D.** Instantaneous planar measurements of velocity and large-scale vorticity and strain rate in an engine using particle image velocimetry. SAE paper 890616, 1989.
21 **Reuss, D. L., Bardsley, M., Felton, P. G., Landreth, C. C.** and **Adrian, R. J.** Velocity, vorticity, and strain rate ahead of a flame measured in an engine using particle image velocimetry. SAE paper 900053, 1990.
22 **Lee, J.** and **Farrell, P. V.** Intake valve flow measurements of an IC engine using particle image velocimetry. SAE paper 930480, 1993.

23 **Nino, E., Gajdeczko, B. F.** and **Felton, P. G.** Two-colour particle image velocimetry in an engine with combustion. SAE paper 930872, 1993.

24 **Reeves, M., Garner, C. P., Dent, J. C.** and **Halliwell, N. A.** Particle image velocimetry measurements of barrel swirl in a production geometry optical IC engine. In Proceedings of SAE Congress and Exposition, Detroit, Michigan, 1994, paper 940281, 1994.

25 **Reeves, M., Garner, C. P., Dent, J. C.** and **Halliwell, N.A.** Study of barrel swirl in a four-valve optical IC engine using particle image velocimetry. In Proceedings of COMODIA 94 International Symposium on *Combustion Diagnostics and Modelling in IC Engines*, Yokohama, Japan, July 1994, pp. 429–435.

26 **Reeves, M., Garner, C. P., Dent, J. C.** and **Halliwell, N. A.** Particle image velocimetry measurements of in-cylinder flow in a multi-valve I.C. engine. *Proc. Instn Mech. Engrs, Part D, Journal of Automobile Engineering*, 1996, **210**(D1), 63–70.

27 **Rouland, E., Trunité, M., Dionnet, F., Floch, A.** and **Ahmed, A.** Particle image velocimetry measurements in a high tumble engine for in-cylinder flow analysis. SAE paper 972831, 1997.

28 **Hinsch, K. D.** Particle image velocimetry. In *Speckle Metrology* (Ed. R.S. Sirohi), 1993 (Marcel Dekker).

29 **Grant, I.** Particle image velocimetry: a review. *Proc. Instn Mech. Engrs, Part C, Journal of Mechanical Engineering Science*, 1997, **211**(C1), 55.

30 **Towers, D. P., Buckberry, C. H.** and **Reeves, M.** Development of a 2 Colour PIV system for in-cylinder spark ignition engine flows. In Proceedings of 9th International Symposium on *Application of Laser Technology to Fluid Mechanics*, Session: Engines-I, Lisbon, Portugal, 1998.

31 **Reeves, M., Towers, D., Tavender, B.** and **Buckberry, C.** A high-speed all-digital technique for cycle-resolved planar flow measurement and flow visualisation within SI engine cylinders. Submitted to *Optics and Lasers in Engng*, December 1998.

32 **Chapman, J., Garrett, M. W.** and **Warburton, A.** A new standard for barrel swirl movement. In Proceedings of IMechE Seminar on *The Heat of the Matter: Gasoline Combustion: Autotech 1991*, Birmingham, 12–15 November 1991, paper C427/18/156.

33 **Reeves, M.** PhD thesis, Loughborough University, 1995.

34 **Lawson, N. J.** The application of particle image velocimetry to high speed flows. PhD thesis, Loughborough University, 1995.

35 **Hocker, R.** and **Kompenhans, J.** Application of particle image velocimetry to transonic flows. In Proceedings of 5th International Symposium on *Application of Laser Technology to Fluid Mechanics*, Lisbon, Portugal, 1990.

36 **Ikeda, Y., Nishigaki, M., Ippommatsu, M., Hosokawa, S.** and **Nakajama, T.** Optimum seeding particles for successful LDV measurements. In Proceedings of 6th International Symposium on *Application of Laser Technology to Fluid Mechanics*, Lisbon, Portugal, 1990.

37 **Kohler, J., Gerblich, K., Meinhardt, P.** and **Ziegler, G. F. W.** 2-D flow velocity measurements under the condition of high straylight intensity using particle tracking anemometry. In Proceedings of International Symposium on *Engineering Turbulence Modelling and Measurements*, Dubrovnik, Croatia, 1990.

38 **Stolz, W., Kohler, J., Lawrenz, W., Meier, F., Bloss, W. H., Maly, R. R., Herweg, R.** and **Zahn, M.** Cycle resolved flow field measurements using a PIV movie technique in a SI engine. In Proceedings of SAE International Fuels and Lubricants Meeting and Exposition, San Francisco, California, October 1992, paper 922354.

39 **Coupland, J. M., Pickering, C. D.** and **Halliwell, N. A.** Particle image velocimetry: theory of directional ambiguity removal using holographic image separation. *Appl. Optics*, 1987, **26**(9).

40 **Gross, L. P., Post, M. E., Trump, D. D.** and **Sarka, B.** Two color particle image velocimetry. ICALEO '89. *LIA Proc.*, 1989, **68**, 101–111.

41 **Lawson, N. J., Reeves, M., Coupland, J. M.** and **Halliwell, N. A.** Particle image velocimetry: image labelling using encoding of the point spread function by application of a polarization sensitive pupil mask. *Appl. Optics*, 1995, **34**(1), 194–200.

42 **Adrian, R. J.** Image shifting technique to resolve directional ambiguity in double-pulsed velocimetry. *Appl. Optics*, 1986, **25**(21).

43 **Landreth, C. C.** and **Adrian, R. J.** Electrooptical image shifting for particle image velocimetry. *Appl. Optics*, 1988, **27**(20).

44 **Lourenco, L. M.** Particle image velocimetry: photographic and video techniques. Von-Karmen Institute Lecture Series on *Laser Velocimetry*, Rhode Saint Genese, Belgium, June 1991.

45 **Wormell, D. C.** and **Sopchak, J. L.** A particle image velocimetry system using a high resolution CCD camera. In Proceedings of IMechE Conference on *Optical Methods and Data Processing in Heat and Fluid Flow*, City University, London, April 1994, paper C485/014.

46 **Keane, R. D.** and **Adrian, R. J.** Theory of cross-correlation analysis of PIV images. *J. Appl. Sci. Res.*, 1992, **49**, 191–215.

47 **Keane, R. D.** and **Adrian, R. J.** Optimisation of particle image velocimeters. Part 1: double pulsed systems. *Measmt Sci. Technol.*, 1990, **1**, 1202–1215.

48 **Reuss, D. L.** and **Rosalik, M. E.** PIV measurements during combustion in a reciprocating internal combustion engine. In Proceedings of 9th International Symposium on *Application of Laser Technology to Fluid Mechanics*, Session: Engines-I, Lisbon, Portugal, 1998.